Research in Astronomy and Astrophysics, 23:115010 (6pp), 2023 November https://doi.org/10.1088/1674-4527/acee53

Prediction for the Multi-band Afterglows of FRB 200428 and its Implication

Mei Du[1], Shuang-Xi Yi[1], Can-Min Deng[2], and Pei Wang[3]
[1] School of Physics and Physical Engineering, Qufu Normal University, Qufu 273165, China; yisx2015@qfnu.edu.cn
[2] Guangxi Key Laboratory for Relativistic Astrophysics, School of Physical Science and Technology, Guangxi University, Nanning 530004, China
dengcm@gxu.edu.cn
[3] National Astronomical Observatories, Chinese Academy of Sciences, Beijing 100101, China
Received 2023 May 23; revised 2023 July 19; accepted 2023 July 21; published 2023 October 4

Abstract

The physical mechanism of fast radio bursts (FRBs) is still unknown. On 2020 April 28, a special radio burst, FRB 200428, was detected and believed to be associated with the Galactic magnetar SGR 1935+2154. It confirms that at least some of the FRBs were generated by magnetars, although the radiation mechanism continues to be debated. To this end, we study in detail the multiband afterglows of FRB 200428 described by the synchrotron fireball shock model. We find the prediction for the optical and radio afterglows of FRB 200428 is consistent with the observations when considering the post-FRB optical and radio upper limits from the literature. We also show that the follow up detection of the afterglows from fast radio bursts like—FRB 200428 is possible at the radio band, though challenging. Based on our model, one can obtain information about the energy of the fireball, the radiation zone, and the nature of the surrounding medium. That may shed light on the physical mechanism of FRBs.

Key words: stars: magnetars – (stars:) gamma-ray bursts: general – radiation mechanisms: non-thermal

1. Introduction

Fast radio bursts (FRBs) are cosmological radio transient sources whose physical origins are still under debated (e.g., Cordes & Chatterjee 2019; Petroff et al. 2019; Zhang 2020; Xiao et al. 2021). On 2020 April 28, a bright radio burst with millisecond duration from the Milky Way magnetar SGR 1935 +2154 was detected simultaneously by the Canadian Hydrogen Intensity Mapping Experiment (CHIME) and Survey for Transient Astronomical Radio Emission 2 (STARE2; e.g., Bochenek et al. 2020; CHIME/FRB Collaboration et al. 2020). With an energy of $\sim 10^{35}$ erg, it is considered likely to be an extension of the extragalactic FRBs at the lower energy end (e.g., Lu et al. 2020). If this radio burst is indeed an FRB (FRB 200428), it directly confirms that at least some of the FRBs were produced by magnetar flares (e.g., Lyubarsky 2014; Beloborodov 2017; Margalit et al. 2018; Metzger et al. 2019).

Due to the more comprehensive data available on repeated FRBs, some theoretical models about the FRB generation mechanism are proposed. Beloborodov (2017) explains the mechanism of repeated FRBs, he suggests that a young magnetar star releases energy from successive flares, the flares are driven by accelerated ambipolar diffusion in the neutron star core, and then power the nebula particles to produce bright millisecond bursts. The energy supply of successive flares and the collision between different flares give rise to a series of repeated FRBs with different intervals. This powerful shock wave can also produce bright optical radiation (e.g., Beloborodov 2020). Yang et al. (2019) studied the brightness and detection prospect of "fast optical bursts" (FOBs) associated with FRBs, indicating that it is possible to detect the associative FOBs in some special inverse Compton scattering processes and with telescopes which with high sensitivity. However, Waxman (2017) put strict constraints on the nature of the persistent source and found that the typical magnetar star wind nebula model is not consistent with the predicted results and a strong synchronous maser emission mechanism adapted to the GHz band is proposed. However, Waxman (2017) found that the typical magnetar wind nebulae model did not agree with the predicted results by placing strict constraints on the properties of the persistent source, so they proposed that the strong synchronous maser emission mechanism could be adapted to the GHz band. Metzger et al. (2019) suggested that the repeated FRBs might be formed by the magnetar-powered synchrotron maser shock model, where the central engines released clean ultrarelativistic magnetization shock waves spread outward, and then the shock colliding with the upstream mildly relativistic magnetized ion-electron shell. The shell through the reverse and forward shock wave to decelerate, the latter of which produces the observed FRBs by synchronous maser mechanism. Similar to GRBs afterglow, the forward shock also heats electrons to extremely relativistic temperatures, powering (incoherent) synchrotron X-ray/gamma-ray emission. Recently, Cooper et al. (2022) have predicted the multi-band afterglow of FRB 200428 based on the magnetar-powered synchrotron maser shock model. In particular, the mechanism of FRB 200428 may be consistent with the previously predicted model, but due to its lower luminosity, the energy distribution may be slightly different (e.g., Wang et al. 2020).

Another breakthrough in the observation of FRB 200428 was that the X-ray burst associated with it was simultaneously detected, with an energy ratio of the radio burst to the X-ray bursts $\sim 10^{-5}$ (e.g., Mereghetti et al. 2020; Li et al. 2021; Ridnaia et al. 2021; Tavani et al. 2021). Incredibly, the far-away model has predicted the occurrence of X-ray burst associated with the FRB, as well as the low radiation efficiency of the FRB ($\sim 10^{-5}$), which was well verified in the case of FRB 200428 (e.g., Margalit et al. 2020). However, recently Wu et al. (2020) found that the ejected baryon matter of the magenta mainly provided by the crust, is higher than the typical mass of a magnetar outer crust. This finding indicates that the outer crust of the magnetar predicted in their model cannot eject enough baryonic mass. We note that the physical mechanism and the rate of the baryonic mass ejection remain uncertain. Thus we suggest that further investigations in observation and theory are required. The close-in model can also account for the low radiative efficiency of FRB 200428 and its associated X-ray bursts, although they were not predicted by the model (e.g., Lu et al. 2020).

Surprisingly, despite numerous X-ray bursts during the SGR 1935+2154 active period, no other FRB event has been detected so far, except for FRB 200428 (e.g., Lin et al. 2020; Bailes et al. 2021; Kirsten et al. 2021). One noticed that the spectrum of the X-ray burst associated with FRB 200428 seems to be much harder than other bursts, with a peak energy $\sim$85 keV (e.g., Ridnaia et al. 2021). This may imply that the X-ray burst associated with FRB 200428 was an unusual burst, and FRBs were produced only in this kind of bursts. It thus leads to speculation that this may be the underlying reason why other X-ray bursts do not have FRB associations. As suggested by Ioka (2020), the usual X-ray bursts could come from the fireballs trapped in the closed field lines of the magnetar, in analogy to the standard model for soft gamma-ray repeaters (SGRs; e.g., Thompson & Duncan 1995, 2001; Kaspi & Beloborodov 2017). However, the X-ray burst associated with the FRB 200428 may come from the trapped-expanding fireball located in the open field line region of the magnetar (e.g., Ioka 2020). The observed temperature of such the expanding fireball remains constant due to relativistic effects, which is consistent with the burst having a larger $E_p \sim 85$ keV than the usual bursts.

As one can see in the physical picture above, the X-ray bursts associated with FRB could be accompanied by energetic ejecta (the expanding fireballs), while the usual X-ray bursts are not. According to the standard fireball model, a pair of shocks will be generated when the fireball sweeps the surrounding medium, including the reverse shock that propagates through the ejecta and the forward shock that propagates through the surrounding medium. Similar to the case of gamma-ray bursts (GRBs), these shocks would produce multiband afterglows (e.g., Yi et al. 2014). The evolution of the afterglows are closely related to the energy of the fireball and the nature of the surrounding environment (e.g., Yi et al. 2014; Zhang 2014). Therefore, when FRB 200428 repeats again in the future, if its multiband afterglows are observed, it will provide new insights into the physical mechanism of FRBs.

In this work, we study in detail the multiband afterglows of FRB 200428, and its detectability. It can be seen that there are many models that attempt to explain the origin of FRBs. It is too early to say which is correct, given the observational evidence so far. Therefore, this work does not attempt to discuss the framework of any specific FRB model. We refer to the afterglow model of GRB and use a memoryless fireball to calculate the afterglow of fast radio bursts. Based on such a model-independent afterglow model, on the one hand, one can predict the timescale and brightness of the afterglow of FRB 200428 that may occur again in the future according to several limited parameters, so as to provide a theoretical basis for afterglow observation. On the other hand, future afterglow observations can be based on our model to make model-independent constraints on the surrounding environment of FRB 200428, which is critical for revealing the physical mechanism of FRB 200428.

This work is organized as follows. The standard afterglow external shock model is described in Section 2 and the results of multifrequency afterglows for FRB 200428 are shown in Section 3. The discussion and conclusion are listed in Section 4.

2. The Model

Following the previous study of Yi et al. (2014), we applied the standard afterglow external shock synchrotron emission model of GRBs (e.g., Mészáros & Rees 1997; Sari et al. 1998; Gao et al. 2013; Yi et al. 2014) to FRBs. This model describes the interaction between the outflow and the ambient medium, and it has several free parameters: the total kinetic energy E, the number density of the ambient medium n_0, the initial Lorentz factor Γ, the shock energy equipartition parameters ε_e and ε_B for electrons and magnetic fields, respectively, and the electron injection spectral index p. If the forward and reverse shocks are both considered, the equipartition parameters ε_e and ε_B and p may be different, so there will be nine parameters.

We mainly consider the forward shock (FS) emission. However, an uncertain phenomenon is whether the reverse shock (RS) emission appeared, which depends on a magnetization parameter of the outflow σ, and the parameter is the ratio between the Poynting flux and the matter flux (e.g., Zhang & Kobayashi 2005; Mimica et al. 2009; Mizuno et al. 2009). Considering FRB 200428 originates from SGR J1935+2154, the outflow may be magnetized. As the study of the previous (e.g., Komissarov et al. 2009; Granot et al. 2011), the outflow is accelerated by a magnetic pressure gradient, and σ is decreased with the radius, lead to the parameter Γ is increased with the radius. Additionally, there is also an obvious magnetic dissipation in the phase of the FRB emission. Therefore, the value of σ has a lot of uncertainty. If it is already below unity,

the RS emission must be expected (e.g., Zhang et al. 2003; Zhang & Kobayashi 2005; Yi et al. 2014).

For the sake of simplicity, we simply considered the standard synchrotron emission, which is mainly decided by the bulk Lorentz factor Γ and the total kinetic energy E, and neglected other complication factors. Under this model, the light curves evolution are associated with three characteristic frequencies: the minimum synchrotron frequency ν_m, the cooling frequency ν_c, the self-absorption frequency ν_a, and the peak flux of the spectrum $F_{\nu,\max}$ (e.g., Gao et al. 2013; Yi et al. 2014). The deceleration timescale of the thin shell case can be represented as,

$$t_\times \sim \frac{l(1+z)}{2c\Gamma^{8/3}}, \tag{1}$$

where $l = (3E/4\pi n_0 m_p c^2)^{1/3}$ is the Sedov length.

Although the surface dipolar magnetic field strength of the magnetar SGR J1935+2154 is around $B_p \sim 10^{14}G$, the radiation efficiency of FRBs in radio band is lower, and the isotropic energy of FRB may be about 5–6 orders of magnitude less than the total energy. According to the observations, the isotropic energy of FRB 200428 is about $\sim 10^{35}$ erg, therefore we apply the total kinetic energy E to be 10^{40} and 10^{41} erg in this work. Additionally, the bulk Lorentz factor of FRB 200428 is adopted as a conservative value 50. Even if we set the Lorentz factor to 100, the brightness of the multi-band afterglows almost has no change (e.g., Falcke & Rezzolla 2014; Katz 2014). The deceleration time is much shorter than the general GRBs, applying the parameters of $E = 10^{41}$ erg, $n_0 = 1$ cm^{-3}, $\Gamma = 50$, the deceleration time of FRB 200428 is approximately $\sim$0.1 s.

Based on the standard assumption (e.g., Sari et al. 1998; Wu et al. 2003; Gao et al. 2013; Yi et al. 2013, 2014, 2020), we can calculate the FRB afterglow emissions. As FRB 200428 is a Galactic transient with the luminosity distance of $\sim$10 kpc (e.g., Zhong et al. 2020), the FS emission of FRB 200428 can be represented at the shock crossing time $t_\times$ as,

$$\nu^f_{m,\times} = 4.1 \times 10^{16} \varepsilon^{1/2}_{B,f,-2} \varepsilon^2_{e,f,-1} n_0^{1/2} \Gamma_2^4 \text{ Hz}, \tag{2}$$

$$\nu^f_{c,\times} = 7.5 \times 10^{23} \varepsilon^{-3/2}_{B,f,-2} n_0^{-5/6} \Gamma_2^{4/3} E_{41}^{-2/3} \text{ Hz}, \tag{3}$$

$$\nu^f_{a,\times} = 4.7 \times 10^{7} \varepsilon^{1/5}_{B,f,-2} \varepsilon^{-1}_{e,f,-1} n_0^{3/5} E_{41}^{1/5} \text{ Hz}, \tag{4}$$

$$F^f_{\nu,\max,\times} = 8.2 \times 10^{-3} \varepsilon^{1/2}_{B,f,-2} n_0^{1/2} E_{41} D_{L,22}^{-2} \text{ Jy}, \tag{5}$$

where $\varepsilon_{e,f} = 0.1$, $\varepsilon_{B,f} = 0.01$ and $p = 2.5$. The evolution of the four parameters during the RS crossing phase (e.g., Mészáros & Rees 1997; Sari et al. 1998; Gao et al. 2013; Yi et al. 2013, 2014),

$$t < t_\times: \nu^f_a \propto t^{\frac{3}{5}}, \nu^f_m \propto t^0, \nu^f_c \propto t^{-2}, F^f_{\nu,\max} \propto t^3, \tag{6}$$

and after the RS crosses,

$$t > t_\times: \nu^f_a \propto t^0, \nu^f_m \propto t^{-\frac{3}{2}}, \nu^f_c \propto t^{-\frac{1}{2}}, F^f_{\nu,\max} \propto t^0. \tag{7}$$

Different from GRBs, due to the FRBs total energy is lower, the outflow will rapidly reach the non-relativistic phase, so the dynamics evolution will have different forms. The transition time appears when the bulk Lorentz factor $\Gamma - 1 = 1$, here $\Gamma \sim (3E/32\pi n_0 m_p c^5 t^3)^{1/8}$. The evolution of the four parameters in this phase can be shown as,

$$\nu^f_a \propto t^{\frac{6}{5}}, \nu^f_m \propto t^{-3}, \nu^f_c \propto t^{-\frac{1}{5}}, F^f_{\nu,\max} \propto t^{\frac{3}{5}}. \tag{8}$$

The transition time at the non-relativistic phase for FRB 200428 afterglow is roughly $t_N \sim 306.1$ s and 659.5 s with $E = 10^{40}$ and 10^{41} erg, respectively.

If an obvious RS emission exists, the four parameters ν^r_m, ν^r_c, ν^r_a, and $F^r_{\nu,\max}$ of the RS at $t_\times$ can be written as:

$$\nu^r_{m,\times} = 1.3 \times 10^{13} \varepsilon^{1/2}_{B,r,-1} \varepsilon^2_{e,r,-1} n_0^{1/2} \Gamma_2^2 \text{ Hz}, \tag{9}$$

$$\nu^r_{c,\times} = 2.4 \times 10^{22} \varepsilon^{-3/2}_{B,r,-1} n_0^{-5/6} \Gamma_2^{4/3} E_{41}^{-2/3} \text{ Hz}, \tag{10}$$

$$\nu^r_{a,\times} = 4.5 \times 10^{10} \varepsilon^{1/5}_{B,r,-1} \varepsilon^{-1}_{e,r,-1} n_0^{3/5} \Gamma_2^{8/5} E_{41}^{1/5} \text{ Hz}, \tag{11}$$

$$F^r_{\nu,\max,\times} = 2.6\, \varepsilon^{1/2}_{B,r,-1} n_0^{1/2} \Gamma_2 E_{41} D_{L,22}^{-2} \text{ Jy}. \tag{12}$$

Due to the outflow is magnetized, the $\varepsilon_{B,r}$ is normalized to 0.1.

The evolution of the four parameters of RS before and after the crossing time can be shown as,

$$t < t_\times: \nu^r_a \propto t^{-\frac{33}{10}}, \nu^r_m \propto t^6, \nu^r_c \propto t^{-2}, F^r_{\nu,\max} \propto t^{\frac{3}{2}}, \tag{13}$$

and

$$t > t_\times: \nu^r_a \propto t^{-\frac{102}{175}}, \nu^r_m \propto t^{-\frac{54}{35}}, \nu^r_c \propto t^{-\frac{54}{35}}, F^r_{\nu,\max} \propto t^{-\frac{34}{35}}. \tag{14}$$

2.1. Results

As the model prediction calculated, the theoretical multi-wavelength afterglows of FRB 200428 are shown in Figures 1 and 2, respectively. Figure 1 shows the FS afterglow light curves of FRB 200428 in the X-ray (2 keV, panel (a)), optical (R-band, panel (b)), and radio (1 GHz, panel (c)) bands, respectively. Considering different emission efficiencies, we take two different kinetic energy values, i.e., $E = 10^{40}$ erg (black) and 10^{41} erg (blue). The other parameters are taken as the typical values: $\Gamma = 50$, $n_0 = 1$ cm^{-3}, $\varepsilon_{e,f} = 0.1$, $\varepsilon_{B,f} = 0.01$, and $p = 2.5$. Then, we also plotted the sensitivity lines of four different detectors in different energy bands, as mentioned in our previous study (e.g., Yi et al. 2014). The rad dash line in panel (a) is the detector sensitivity line of Swift/XRT, which is $\propto t^{-1}$ early on and breaks to $\propto t^{-1/2}$ when $F_\nu = 2.0 \times 10^{-15}$ erg cm^{-2} s^{-1} at $t = 10^5$s (e.g., Moretti et al. 2009; Yi et al. 2014). The green dashed line in panel (a) is the sensitivity line of the Insight-HXMT, which scales as $\propto t^{-1}$ for arbitrarily long exposure times. The red dashed line in panel (b) is the sensitivity line of the Large Synoptic Survey Telescope (LSST) Array. In the survey model, LSST reaches 24.5 mag in 30 s. The red dashed line in panel (c) is the sensitivity line of the Expanded Very Large Array (EVLA), which scales as $\propto t^{-1/2}$ for arbitrarily long exposure times.

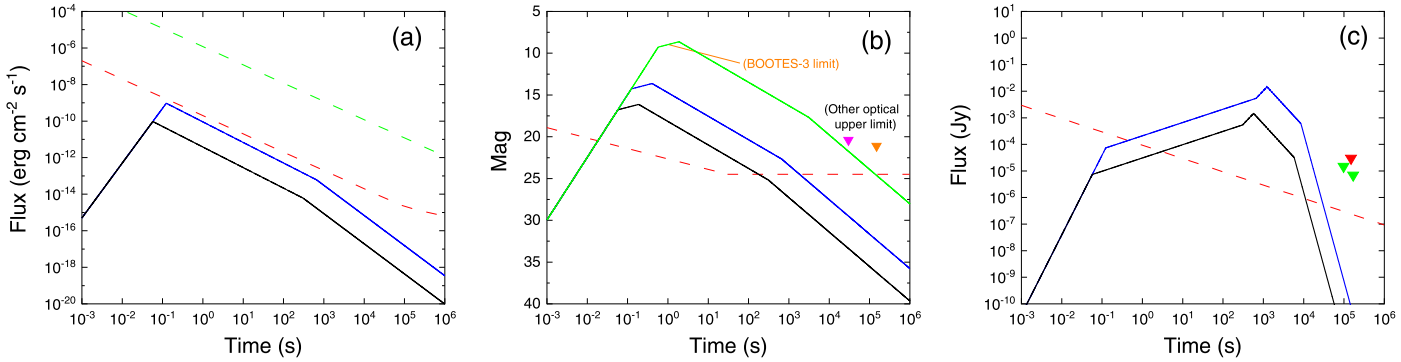

Figure 1. Example forward shock afterglow light curves of FRB 200428. The model parameters: $\epsilon_{B,f} = 0.01$, $\epsilon_e = 0.1$, $n_0 = 1$, $p = 2.5$, and $\eta = 50$. Three values of the energy $E = 10^{40}$ (black), 10^{41} (blue) and 10^{43} (green, only in the optical band) have been adopted. (a) The X-ray light curves at 2 keV. The red dashed line is the detector sensitivity line of Swift/XRT, and the green dashed line is the detector sensitivity line of Insight-HXMT. (b) *R*-band light curves. The red dashed line is the detector sensitivity line of LSST. The orange line is the optical upper limits taken from Cooper et al. (2022), and the blue (*R*-band) and orange (*z*-band) triangle points are the optical upper limits from LCOGT and BOOTES-2 (Lin et al. 2020), respectively. (c) Radio light curves at 1 GHz. The red dashed line is the detector sensitivity line of VLA. The green (1.36 GHz) and red (6 GHz) points are the radio upper limits by Effelsberg and VLA (Bailes et al. 2021), respectively.

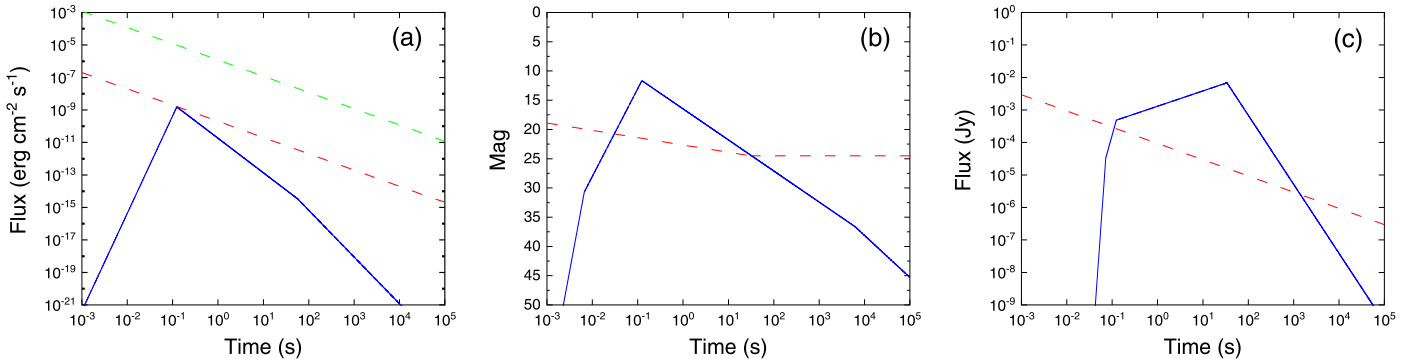

Figure 2. Example reverse shock afterglow light curves of FRB 200428. The model parameters: $\epsilon_{B,r} = 0.16$, $\epsilon_e = 0.1$, $n_0 = 1$, $p = 2.5$, and $\eta = 50$. The energy $E = 10^{41}$ (blue solid line) has been applied. The different detector sensitivity lines are the same as shown in Figure 1.

As shown in Figure 1 panel (a), the X-ray afterglow of FRB 200428 is too faint, theoretically neither the Swift/XRT nor Insight-HXMT can detect its X-ray afterglow. Considering the first X-ray counterpart of FRB 200428 was observed, Insight-HXMT implemented a long time observation of SGR J1935 +2154 since then. Still, no X-ray counterparts from FRB 200428 were detected, only hundreds of short X-ray bursts triggered by Insight-HXMT and a series of other astronomical satellites were obtained (e.g., Cai et al. 2022). In the optical *R* band (panel (b)), the peak magnitude is about 16 and 13.6 for the energies $E = 10^{40}$ and 10^{41} erg, respectively. We can see the sensitivity line of LSSA is below the peak magnitude. However, due to the very early peak time of ∼0.2–0.4 s, which lead the LSSA cannot follow up quickly. For optical bands, it is still possible to detect the counterpart emission if follow-up observations are performed within a few hundred seconds after FRB occurs. In the 1 GHz radio band (panel (c)), the peak flux density is about 1.46×10^{-3} and 1.46×10^{-2} Jy, the peak time is about $\sim 5.7 \times 10^2$ and 1.2×10^3 s for two different kinetic energies, respectively. This might be caught by EVLA if followed up early. Regrettably, the EVLA did not detect this source during this period. As reported by Bailes et al. (2021), after about 4×10^4 s of FRB 200428 triggered, the radio telescope MeerKAT started to point to the source. However, they did not detect any signals, due to the flux of the FS emission declining rapidly or the diffuse emission around the magnetar. Compared with other energy bands, the radio afterglows from FRBs are the most promising to be detected, mainly because the radio afterglows last a very long time. Therefore, if we are lucky enough to detect a bonafide FRB like-FRB 200428 again, rapid radio observations on minutes to several hours timescales will be the best opportunity to observe the afterglows.

The RS emission for FRB 200428 is also shown in Figure 2. Fixing other parameters, we allow the total energy $E = 10^{41}$ erg and $\varepsilon_{B,r} = 0.16$. In general, the RS afterglow of FRB 200428 is

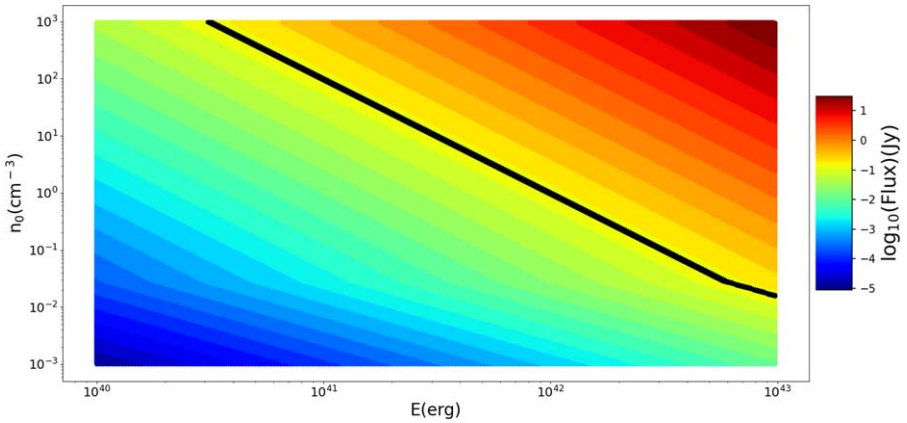

Figure 3. Contour of optical peak flux in the E–n_0 plane. Different colors mean different optical peak flux, and the solid line represents peak flux for 0.1 Jy which is the BOOTES-3 upper limit. The black line represents the limitation on the model parameter space imposed by the observation upper limit of BOOTES-3.

more difficult to be detected by current detectors. Either the afterglow emission is too faint, or it peaks too early. As shown in Figure 2, like the FS emission, the RS X-ray afterglow (panel (a)) is too faint, however the peak time of the optical R-band (panel (b)) is so early ($t_p \sim 0.1$ s) for the LSST. Additionally, the 1 GHz radio band of FRB 200428 (panel (c)) can reach the peak flux early ($\sim$33 s) but rapidly declines.

According to Cooper et al. (2022), who have provided optical lightcurves using the method from Margalit et al. (2020), and applied the BOOTES-3 upper limits to constrain the FRB afterglow significantly. They supposed that the optical flux limit scales as $F_{\rm limit} \propto t^{-1/2}$ and started with early observations (the orange line). We also used the same energy $E = 1 \times 10^{43}$ erg in our afterglow model, the estimated results (the green line in panel (b) of Figure 1) almost reach the optical upper limits. Our optical results are also consistent with the prediction from Cooper et al. (2022). To better show how optical peak flux depends on E and n_0, we give the contour of optical peak flux in the E–n_0 space in Figure 3. We set $\epsilon_{B,f} = 0.01$, $\epsilon_e = 0.1$, $p = 2.5$ and $\eta = 50$, but the energy with a range of 10^{40}–10^{43} erg and n_0 with a range of 10^{-3}–10^{3} cm^{-3}. The reasonable parameter space of FRB 200428 may be reflected by the optical observation upper limits from the contour of peak flux. As shown in the figure, the black line represents the limitation on the model parameter space imposed by the observation upper limit of BOOTES-3. It is easy to see from the contour that only when the environment around FRB 200428 is dense enough, it is possible to produce sufficiently bright radio afterglows.

3. Summary and Discussion

In this work, we applied the standard afterglow external shock synchrotron emission model of GRBs to the peculiar case of FRB 200428, and calculated its multi-wavelength afterglows. As a result, we found that owing to its low energy, the broad-band afterglows of FRB 200428 are very faint. Even so, current detectors may be able to follow up and detect its broad-band afterglows, especially at radio wavelengths.

The X-ray afterglow emitted from FS is so weak and decays rapidly after the peak that it is hard for current detectors to catch. This may require a wide-field XRT (such as the Einstein Probe or Lobster), and it may have a chance of capturing the X-ray afterglow of FRB 200428 in the future, when FRB 200428 repeats. For the optical afterglow, the current detectors can only pick it up theoretically, because it is difficult to follow up quickly due to the early peak and the fast decay. The most optimistic afterglow of FRB 200428 was found in the radio band, although the radio afterglow flux only reached the mJy level. Thanks to the relatively late peaking time of the radio afterglow ($\sim 10^3$ s), if the radio telescopes can move to the source position within an hour, there is a good chance of catching it. In general, follow up detection of the afterglow from the FS of FRB 200428 is plausible, though challenging. In contrast, the afterglow from RS is almost impossible to be detected by current detectors, either the emission is too weak or it peaks too early. Given the difficulty of follow-up observation, the strategy of long-term observation when SGR 1935 +2154 enters the active phase may be adopted. In this way, the chance of catching the afterglow is much greater, but much more observation time is required.

Cooper et al. (2022) also estimated the multi-wavelength afterglows of FRB 200428, based on the model of Metzger et al. (2019). They provided results from LOFAR imaging observations of SGR 1935+2154. Due to its low luminosity, the predicted multi-band afterglows from FRB 200428 are still too faint to be detected, and placing some radio and optical upper limits in the afterglow emissions (also see the upper limits in our results). Considering the similarity of the early afterglow models, our results are very consistent with the predictions of Cooper et al. (2022), especially considering the

same parameters for this burst. In any case, one can imagine that once the afterglow of fast radio bursts like-FRB 200428 is observed in the future, based on the early afterglow model, one can obtain information about the energy of the fireball, the radiation zone and the nature of the surrounding medium. That may shed light on the physical mechanism of FRBs.

Note: Interestingly, since 2022 October 10, SGR J1935 +2154 is active again (e.g., Ryder et al. 2022) and a radio burst was detected from it associated with an X-ray burst (e.g., Dong & CHIME/FRB Collaboration 2022; Wang et al. 2022), proving another case that magnetars can drive FRBs. In order to search for additional FRB-magnetar burst associated cases and search for radio pulsations (e.g., Zhu et al. 2020), four FAST observations have been done on SGR J1935+2154, but no pulses are detected. We also propose four NICER observations on SGR J1935+2154 simultaneous with FAST, to cover a possible magnetar burst in soft X-ray, and search for possible correlated radio/X-ray pulsation, still no pulses are detected. On 2022 October 22, a radio burst was detected (e.g., Huang et al. 2022) from *S*-band 40 m Yunnan telescope, CAS. Time of *S*-band burst (MJD): 59873.417891687764495, 2020-10-21 18:01:45 (UT+8), this arrival time of the radio burst is well consistent with an HXMT X-ray outburst (e.g., Li et al. 2022), the arrival time delay between radio and X-ray can be ignored within the error. There is no counterpart detected at this stage, and the follow up detection of the multi-band afterglows from FRBs is challenging.

Acknowledgments

This work is supported by the National Natural Science Foundation of China (grant No. U2038106), and China Manned Spaced Project (CMS-CSST-2021-A12). C.M.D. is supported by the National Natural Science Foundation of China (grant No. 12203013), and the Guangxi Science Foundation (grant Nos. AD22035171 and 2023GXNSFBA026030).

References

Bailes, M., Bassa, C. G., Bernardi, G., et al. 2021, MNRAS, 503, 5367
Beloborodov, A. M. 2017, ApJL, 843, L26
Beloborodov, A. M. 2020, ApJ, 896, 142
Bochenek, C. D., Ravi, V., Belov, K. V., et al. 2020, Natur, 587, 59
Cai, C., Xiong, S.-L., Lin, L., et al. 2022, ApJS, 260, 25
CHIME/FRB Collaboration, Andersen, B. C., Bandura, K. M., et al. 2020, Natur, 587, 54
Cooper, A. J., Rowlinson, A., Wijers, R. A. M. J., et al. 2022, MNRAS, 517, 5483
Cordes, J. M., & Chatterjee, S. 2019, ARA&A, 57, 417
Dong, F. A. & CHIME/FRB Collaboration 2022, ATel, 15681
Falcke, H., & Rezzolla, L. 2014, A&A, 562, A137
Gao, H., Lei, W.-H., Zou, Y.-C., et al. 2013, NewAR, 57, 141
Granot, J., Komissarov, S. S., & Spitkovsky, A. 2011, MNRAS, 411, 1323
Huang, Y. X., Xu, H., Xu, Y. H., et al. 2022, ATel, 15707
Ioka, K. 2020, ApJL, 904, L15
Kaspi, V. M., & Beloborodov, A. M. 2017, ARA&A, 55, 261
Katz, J. I. 2014, PhRvD, 89, 103009
Kirsten, F., Snelders, M. P., Jenkins, M., et al. 2021, NatAs, 5, 414
Komissarov, S. S., Vlahakis, N., Königl, A., et al. 2009, MNRAS, 394, 1182
Li, C. K., Lin, L., Xiong, S. L., et al. 2021, NatAs, 5, 378
Li, X. B., Zhang, S. N., Xiong, S. L., et al. 2022, ATel, 15708
Lin, L., Zhang, C. F., Wang, P., et al. 2020, Natur, 587, 63
Lu, W., Kumar, P., & Zhang, B. 2020, MNRAS, 498, 1397
Lyubarsky, Y. 2014, MNRAS, 442, L9
Margalit, B., Beniamini, P., Sridhar, N., et al. 2020, ApJL, 899, L27
Margalit, B., Metzger, B. D., Berger, E., et al. 2018, MNRAS, 481, 2407
Mereghetti, S., Savchenko, V., Ferrigno, C., et al. 2020, ApJL, 898, L29
Mészáros, P., & Rees, M. J. 1997, ApJ, 476, 232
Metzger, B. D., Margalit, B., & Sironi, L. 2019, MNRAS, 485, 4091
Mimica, P., Giannios, D., & Aloy, M. A. 2009, A&A, 494, 879
Mizuno, Y., Zhang, B., Giacomazzo, B., et al. 2009, ApJL, 690, L47
Moretti, A., Piotto, G., Arcidiacono, C., et al. 2009, A&A, 493, 539
Petroff, E., Hessels, J. W. T., & Lorimer, D. R. 2019, A&ARv, 27, 4
Ridnaia, A., Svinkin, D., Frederiks, D., et al. 2021, NatAs, 5, 372
Ryder, S. D., Alsaberi, R. Z. E., Anderson, G., et al. 2022, ATel, 15687
Sari, R., Piran, T., & Narayan, R. 1998, ApJL, 497, L17
Tavani, M., Casentini, C., Ursi, A., et al. 2021, NatAs, 5, 401
Thompson, C., & Duncan, R. C. 1995, MNRAS, 275, 255
Thompson, C., & Duncan, R. C. 2001, ApJ, 561, 980
Wang, C. W., Xiong, S. L., Zhang, Y. Q., et al. 2022, ATel, 15682
Wang, W.-Y., Xu, R., & Chen, X. 2020, ApJ, 899, 109
Waxman, E. 2017, ApJ, 842, 34
Wu, Q., Zhang, G. Q., Wang, F. Y., et al. 2020, ApJL, 900, L26
Wu, X. F., Dai, Z. G., Huang, Y. F., et al. 2003, MNRAS, 342, 1131
Xiao, D., Wang, F., & Dai, Z. 2021, SCPMA, 64, 249501
Yang, Y.-P., Zhang, B., & Wei, J.-Y. 2019, ApJ, 878, 89
Yi, S.-X., Gao, H., & Zhang, B. 2014, ApJL, 792, L21
Yi, S.-X., Wu, X.-F., & Dai, Z.-G. 2013, ApJ, 776, 120
Yi, S.-X., Wu, X.-F., Zou, Y.-C., et al. 2020, ApJ, 895, 94
Zhang, B. 2014, ApJL, 780, L21
Zhang, B. 2020, Natur, 587, 45
Zhang, B., & Kobayashi, S. 2005, ApJ, 628, 315
Zhang, B., Kobayashi, S., & Mészáros, P. 2003, ApJ, 595, 950
Zhong, S.-Q., Dai, Z.-G., Zhang, H.-M., et al. 2020, ApJL, 898, L5
Zhu, W., Wang, B., Zhou, D., et al. 2020, ATel, 14084